A Preliminary Study on the Compliant Stretcher Mechanism of Canopy

Sara Lee Kit Yee[1,*], *Lam Yeap* Sheng[1] and *Tan Yong* Li[1]

[1]Center of Systematic Innovation Research, Department of Mechanical Engineering, Faculty of Engineering and Technology, Tunku Abdul Rahman University College, 53300 Kuala Lumpur, Malaysia.

Abstract. The design of the canopy utilizes the conventional rigid body mechanisms which is vulnerable to the presence of backlash, friction of joints or wearing of mechanical parts which lead to short product life. Compliant mechanisms are employed to reduce these mechanical problems, owing to their zero-joint and monolithic structure. A reference design for the conventional canopy was chosen and modified through reviewing different patent designs. Six different configurations of the pseudo-rigid-body model (PRBM) were constructed, and the best configuration was selected. Kinematic synthesis with function generation was performed for the chosen PRBM using MATLAB. The obtained results from the kinematic synthesis were then used to calculate the dimensions and stresses of the flexural pivots for the compliant stretcher mechanism. Finite Element Analysis (FEA) simulation was then performed on each of the models and the obtained flexural pivot stresses were compared with that of the PRBM. This research successfully replaces all the rigid joints and links of the stretcher mechanism of the conventional canopy to form a monolithic structure of compliant stretcher mechanism.

1 Introduction

A conventional canopy mechanism consists of static bodies known as rigid bodies such as a ferrule, runner, ribs that are connected to both the stretchers and the fabric of the canopy, and a main shaft. The design of the canopy utilizes the conventional rigid body mechanisms that consist of linkages and revolute joints, which connected to transmit motion. Since motion of mechanism is transferred through rigid joints and rigid links, the mechanism will be vulnerable to the presence of backlash, friction of joints or wearing of mechanical parts which lead to a shorter product life [1]. On the other hand, compliant mechanisms are known to be monolithic which transmit motion through the deflection of the compliant elements in their structure. Therefore, compliant mechanisms can provide a zero-joint alternative as compared to the conventional rigid body mechanisms, which reduce these tedious mechanical problems [2].

Pseudo-rigid-body model (PRBM) is a commonly known method for modelling compliant mechanisms due to its convenience in analysing and estimating the mobility of the compliant mechanisms. This method provides a framework identical to the conventional rigid body mechanics which analyses the position and orientation of the compliant body conveniently. Howell and Midha [3] proposed a systematic method of utilizing the PRBM for analysis and design of small-length flexural pivots (SLFP). Characteristic pivots are also used to identify the position of pin joints for the PRBM to obtain an accurate prediction of compliant mechanism [4]. Crews et al. [5] mentioned that the PRBM is a well-known method that could accurately predict the deflection of homogenous compliant segments.

Rigid body replacement is one of the recognized methods to synthesise compliant mechanisms which begins with three common cases, an existing rigid body mechanism, a desired task and a compliant mechanism concept. Normally, this approach is used to modify an existing rigid body mechanism through the replacement of rigid links and movable joints with equivalent compliant members to construct different possible configurations of PRBM [2]. Murphy et al. [6] proposed the method of dividing compliant links into segments and introduced the three basic forms of connection for the segments which are known as the rigid body joint or kinematic pair, flexural pivot and fixed connection. There are also some rules set for the types of connection used for different combination of links which are based on the segment compliance content.

In this study, a reference design for the conventional canopy was chosen through reviewing different patent designs. Different configurations of PRBM were constructed to select the best configuration. Kinematic synthesis with function generation was performed for the chosen configuration with the application of MATLAB to obtain the dimensions and flexural pivot stresses for the compliant stretcher mechanism. The final design of the compliant stretcher mechanism was analysed with different materials through Finite Element Analysis (FEA).

2 Methodology

* Corresponding author: leeky@tarc.edu.my

The rigid body model is focused on the canopy frame stretchers as they are responsible for extend and close of the ribs. It can be observed that the movement of the stretcher mechanism is similar to that of the slider-crank mechanism, which is a variation of four-bar mechanism where one of the pivot joints is replaced with a prismatic joint that slides in one direction. The rigid body model of the stretcher mechanism is modelled with all the links and joints labelled as shown in Figure 1. The boundary condition and parameters of the rigid body model are listed out in Table 1.

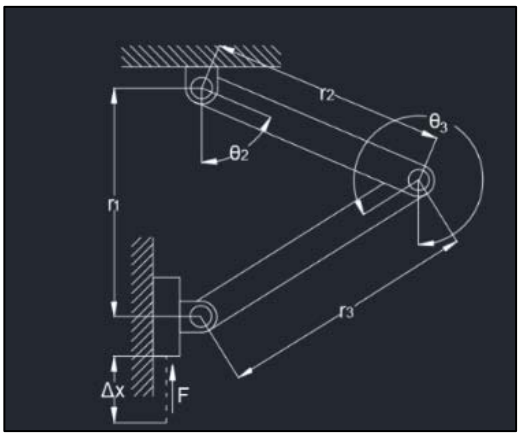

Fig. 1. Rigid body model of the mechanism.

Table 1. Parameters of the rigid body model for stretcher mechanism.

Parameters	Value
Distance of slider from the top hinge, r_1	0.45 m (initial), 0.15 m (extended)
Link 2, r_2	0.20 m
Link 3, r_3	0.25 m
Link angle 2, θ_2	0º (initial), 90º (extended)
Link angle 3, θ_3	0º (initial), 307º (extended)
Maximum displacement of slider, Δx	0.30 m

Figure 2 shows the six PRBM configurations for compliant stretcher mechanism. Design A, B and C consists of rigid links with the combinations of rigid body joint and flexure pivot. On the other hand, design D, E and F consists of rigid link and flexible segment, with a fixed/clamped connection. These designs have the advantage of reducing the part count significantly, but it is constricted by the limited amount of moment and stress that can be applied to the flexible segments. Besides, additional considerations such as buckling and critical load need to be made.

Design A and B are easier to synthesis and analyse as they are partial compliant mechanism and fewer considerations required. However, the part count reduction is not significant for these two designs. Design C is a monolithic compliant mechanism that uses three flexure pivots to replace all the rigid body joints which have the potential in reducing the part count significantly. In this study, design C is selected as the compliant mechanism configurations for the rigid body model.

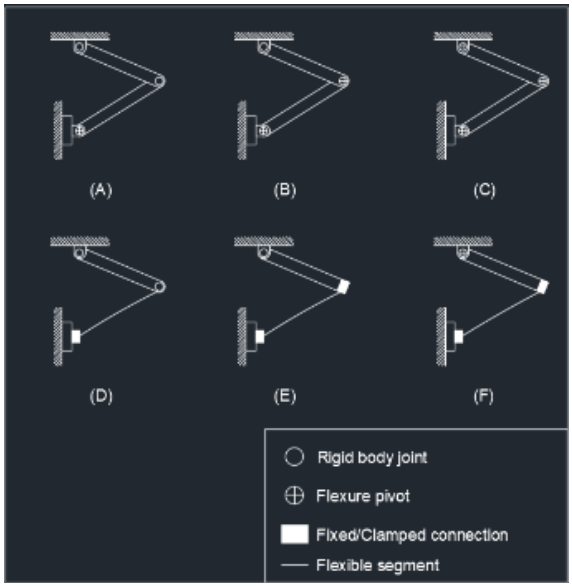

Fig. 2. PRBM configurations of stretcher mechanism.

The link of the compliant mechanism is made up of two different segments where the shorter one is known as small-length flexural pivots (SLFP) that exhibits better flexibility [5]. Theoretically, the length of the large segments should be ten or more times longer than that of the small segment. The motion of the system can be modelled as two rigid links that are joined together by a pin joint known as the characteristic pivot, which is situated at the centre of the flexural pivot [7]. PRBM utilized torsional spring to indicate the deflection resistance of a beam defined by its spring constant, K. The torsional spring constant for the SLFP. Howell [7] stated that the stress experienced by the SLFP can be assumed to correlate with the moment at the SLFP, which is assumed to be nearly constant owing to the relatively short length of the flexural pivots.

The force-deflection relationship for the PRBM slider mechanism can be determined through the application of the principle of virtual work ($\delta W=0$ for equilibrium) [8]. As refer to Figure 3, the total virtual work of the system can be expressed according to Equation (1).

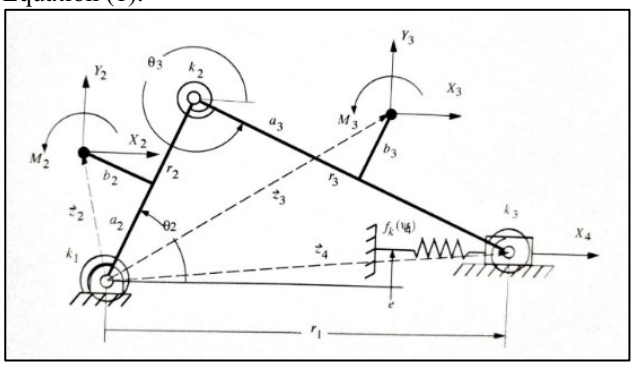

Fig. 3. A general pseudo-rigid-body slider mechanism

$$\delta W = \sum_{i=2}^{4} \overrightarrow{F_i} \cdot \delta\overrightarrow{z_i} + \sum_{i=2}^{3} \overrightarrow{M_i} \cdot \delta\overrightarrow{\theta_i} + \sum_{i=1}^{3} \overrightarrow{T_i} \cdot \delta\overrightarrow{\psi_i} + \overrightarrow{F_s} \cdot \delta\overrightarrow{z_4} \quad (1)$$

where $\overrightarrow{F_i}$ is the force applied to link i, $\overrightarrow{M_i}$ is the moment applied to the link i, $\overrightarrow{T_i}$ is the moment at the characteristic pivot i and $\overrightarrow{F_s}$ is the spring force.

Figure 4 illustrates the PRBM of the compliant stretcher mechanism with defined variables. Since the slider mechanism used for the compliant stretcher mechanism did not utilize any spring, the $\overrightarrow{F_s}$ can be ignored, and the resultant output force of the system as in Equation (2).

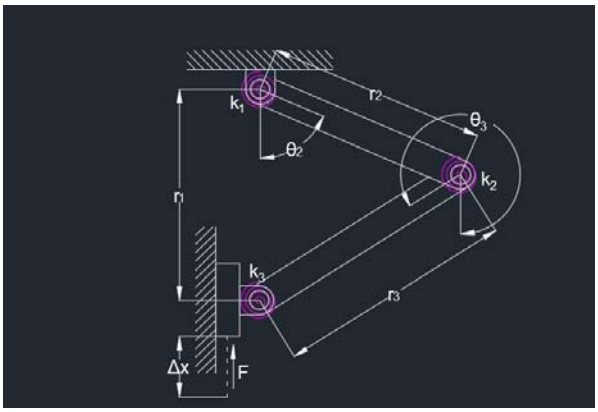

Fig. 4. PRBM of the compliant stretcher mechanism.

$$F = \frac{r_3 \cos\theta_3\{\kappa_1\theta_2+\kappa_2(2\pi+\theta_2-\theta_3)\}}{r_2 r_3 \sin(\theta_2-\theta_3)} + \frac{r_2 \cos\theta_2\{\kappa_2(2\pi+\theta_2-\theta_3)-\kappa_3(2\pi-\theta_3)\}}{r_2 r_3 \sin(\theta_2-\theta_3)} \quad (2)$$

3 Results and Discussion

3.1 Kinematics Synthesis

For the kinematic synthesis of the compliant stretcher mechanism using PRBM, the chosen number of precision positions is five with 14 equations, 19 unknowns and five free choices. The precision position (end position) with the applied force of F_1 to F_4 are written as in Equation (3) to (6).

$$F_1 = \frac{r_3 \cos\theta_{31}\{\kappa_1\theta_{21}+\kappa_2(2\pi+\theta_{21}-\theta_{31})\}}{r_2 r_3 \sin(\theta_{21}-\theta_{31})} + \frac{r_2 \cos\theta_{21}\{\kappa_2(2\pi+\theta_{21}-\theta_{31})-\kappa_3(2\pi-\theta_{31})\}}{r_2 r_3 \sin(\theta_{21}-\theta_{31})} \quad (3)$$

$$F_2 = \frac{r_3 \cos\theta_{32}\{\kappa_1\theta_{22}+\kappa_2(2\pi+\theta_{22}-\theta_{32})\}}{r_2 r_3 \sin(\theta_{22}-\theta_{32})} + \frac{r_2 \cos\theta_{22}\{\kappa_2(2\pi+\theta_{22}-\theta_{32})-\kappa_3(2\pi-\theta_{32})\}}{r_2 r_3 \sin(\theta_{22}-\theta_{32})} \quad (4)$$

$$F_3 = \frac{r_3 \cos\theta_{33}\{\kappa_1\theta_{23}+\kappa_2(2\pi+\theta_{23}-\theta_{33})\}}{r_2 r_3 \sin(\theta_{23}-\theta_{33})} + \frac{r_2 \cos\theta_{23}\{\kappa_2(2\pi+\theta_{23}-\theta_{33})-\kappa_3(2\pi-\theta_{33})\}}{r_2 r_3 \sin(\theta_{23}-\theta_{33})} \quad (5)$$

$$F_4 = \frac{r_3 \cos\theta_{34}\{\kappa_1\theta_{24}+\kappa_2(2\pi+\theta_{24}-\theta_{34})\}}{r_2 r_3 \sin(\theta_{24}-\theta_{34})} + \frac{r_2 \cos\theta_{24}\{\kappa_2(2\pi+\theta_{24}-\theta_{34})-\kappa_3(2\pi-\theta_{34})\}}{r_2 r_3 \sin(\theta_{24}-\theta_{34})} \quad (6)$$

MATLAB software is used to solve Equation (3) to (6) iteratively for this approach and the results are shown in Table 2. Three different sets of results obtained from the kinematic synthesis with three presume values of torsional spring constants K_n, as tabulated in the table. It was observed that the difference between the three sets of presume values are less than 1%. Since the percentage difference among the values is minimal, the three sets of initial presume values could be used.

As refer to Table 2, link 3 angle, θ_{34} is 5.3592 rad, which is 307.01°. This angle is identical to the final deflected angle of the concept design stated in Table 1 (307°), as compared to the other two sets of initial guess values (307.05°). Therefore, the values obtained by the torsional spring constant of 20 N.m/rad are chosen for CAD design in this study.

Table 2. Three different sets of presume values.

Unknown Variables	Solved Values		
	K_n = 20 N.m/rad	**K_n = 15 N.m/rad**	**K_n = 10 N.m/rad**
Spring constant for the 1st joint, κ_1 (N.m/rad)	0.4997	0.5024	0.5020
Spring constant for the 2nd joint, κ_2 (N.m/rad)	0.1082	0.1093	0.1092
Spring constant for the 3rd joint, κ_3 (N/m/rad)	0.1699	0.1717	0.1715
Link 2 angle at 2nd position, θ_{21} (rad)	0.6852	0.6864	0.6863
Link 2 angle at 3rd position, θ_{22} (rad)	0.9401	0.9394	0.9394
Link 2 angle at 4th position, θ_{23} (rad)	1.2983	1.2964	1.2966
Link 3 angle at 2nd position, θ_{31} (rad)	5.7575	5.7569	5.7570
Link 3 angle at 3rd position, θ_{32} (rad)	5.5657	5.5662	5.5662
Link 3 angle at 4th position, θ_{33} (rad)	5.4325	5.4315	5.4317
Link 3 angle at 5th position, θ_{34} (rad)	5.3592	5.3591	5.3591

3.2 Calculation of Stresses of Flexural Pivots

After the kinematic synthesis with function generation, the obtained values are used for the calculation of the dimensions of the flexural pivots and the associated stresses experienced by each flexure pivots as they achieve the desired deflections. From the kinematic synthesis results, the torsional spring constants for each

of the flexural pivots are 0.4997 N.m/rad, 0.1082 N.m/rad and 0.1699 N.m/rad respectively. The length of each of flexural pivots of the stretcher mechanism is set to be 0.01 m.

Three material are evaluated, which are stainless steel (SS) and aluminium alloy (AA) for the actual design, and polyethylene terephthalate (PET) for the scaled-down prototype. The size of the prototype is scaled down to one-fifth of the actual size of the stretcher mechanism for demonstration purpose. The Young's Modulus for SS, AA and PET are 193 GPa, 71 GPa and 2.7 GPa respectively. The thickness of the flexural pivots is calculated using Equation (7), while the flexural pivot stress is calculated using Equation (8). Dimension and flexural pivots stress for different materials is tabulated in Table 3.

$$h_n = \sqrt[3]{\frac{12I_n}{b_n}} \tag{7}$$

$$\sigma_n = \frac{\theta_n E h_n}{2l_n} \tag{8}$$

where n is the nth flexural pivots and n = 1, 2 and 3, I is the moment of inertia, b is base length, h is height, E is Young's modulus and θ is angular deflection,

Table 3. Dimensions and flexural pivots stress for different materials.

Material	Flexural Pivots	Angular Deflection, θ_0 (rad)	Thickness of Flexural Pivots, h (mm)	Flexural Pivot Stress, σ (MPa)
SS	1	1.5708	0.4267	6468.01
	2	5.3582	0.2562	13247.24
	3	0.9250	0.2978	2658.24
AA	1	1.5708	0.5955	3320.71
	2	5.3582	0.3576	6802.13
	3	0.9250	0.4156	1364.73
PET	1	1.5708	1.7707	375.49
	2	5.3582	1.0633	769.15
	3	0.9250	1.2359	154.33

According to Table 3, SS material experienced the highest flexural pivots stress whereas the PET material experienced the lowest stress. This is due to the difference in the values of Young's Modulus for all three materials. Since SS has the highest value of Young's Modulus as compared to AA and PET, higher stress is required for the flexural pivots to achieve the desired deflections. Specifically, second flexural pivot experiences the highest stress as compared with the first and third flexural pivot regardless of the choice of materials. This is because the second flexural pivot has the highest angle of deflection of 5.3582 rad or 307°. This signifies that the flexural pivot will have to experience additional stress to achieve the amount of deflection. It is deduced that the stress experienced by the flexural pivots increases drastically as the angle of deflection of the flexural pivots increases.

3.3 CAD Design of the Mechanism

For the CAD designing of the compliant stretcher mechanism, SolidWorks software is used to design the compliant stretcher mechanism with the values obtained from Table 1 and 3. Since the thickness of the flexural pivots is affected by the Young's Modulus of the material, each of the material used will have a different design in terms of thickness of the flexural pivots. However, the overall design for the actual model is almost identical whereas the prototype design has more significant differences in terms of appearances. Figure 5 and 6 show the CAD design for the actual models and prototype model.

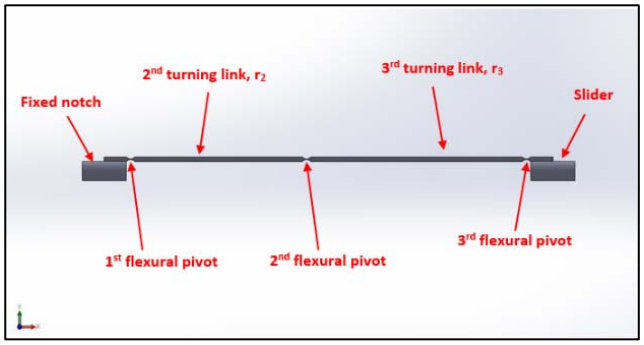

Fig. 5. CAD design for the actual model of the compliant stretcher mechanism for stainless steel and aluminium alloy.

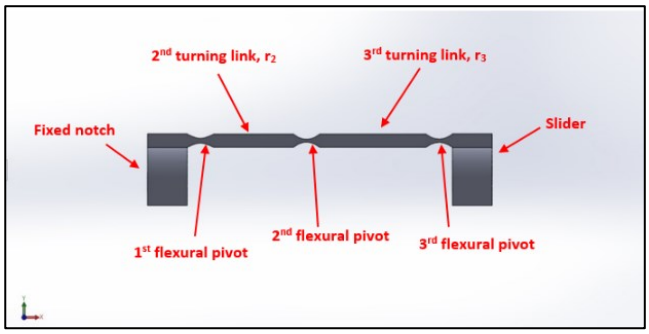

Fig. 6. CAD design for the prototype model with a scale factor of 0.2 using PET.

3.4 Non-Linear Analysis of the Compliant Stretcher Mechanism using FEA

Since the flexural pivots for the compliant stretcher mechanism experienced large deflection, non-linearity characteristics of the mechanism are considered. The non-linear analysis is performed on all three models with different materials for the compliant stretcher mechanism using SolidWorks software. Figure 7 to 9 show the comparison of flexural pivot stresses obtained from PRBM and FEA simulation for the three models.

From the obtained flexural pivot stresses from both the PRBM and FEA simulation, it is noticed that some of

the flexural pivots experience high values of stress, noticeably for the second flexural pivot for all three models. For compliant mechanisms, maximum stress merely occurs at the outer fibres of the flexural pivots for most of the cases according to Howell [7]. Due to the ductile characteristic of the materials chosen for this study, despite the mechanism will yield at that particular point of high-stress concentration, the heavy loads will be eventually redistributing to the adjacent material around the flexural pivots. The resulting plastic deformation will be insignificant. It was found that the flexural pivot stress obtained from the non-linear analysis with FEA method are in close agreement to the PRBM method, which reveals the success of the Rigid body replacement approach in designing the functionality compliant stretcher mechanism.

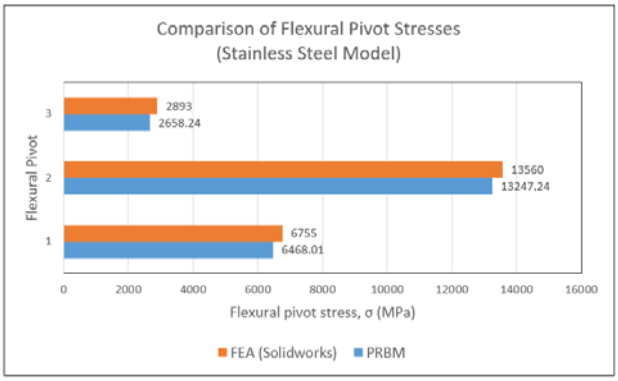

Fig. 7. Comparison of flexural pivot stresses for PRBM and FEA simulation for stainless steel model.

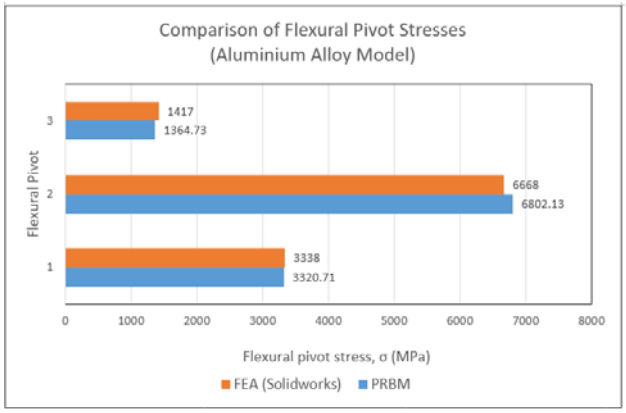

Fig. 8. Comparison of flexural pivot stresses for PRBM and FEA simulation for aluminium alloy model.

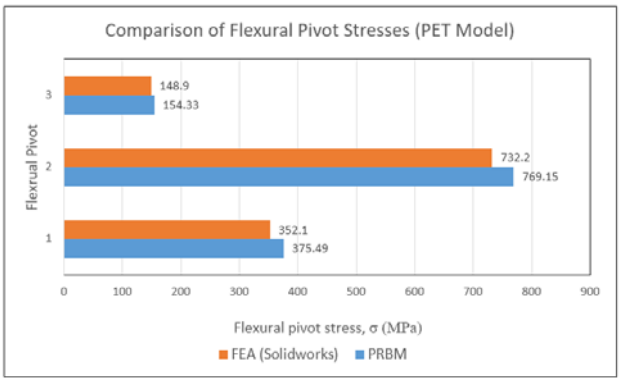

Fig. 9. Comparison of flexural pivot stresses for PRBM and FEA simulation for PET model.

4 Conclusions

The solution obtained from the kinematic synthesis with function generation was concluded to be a satisfactory solution as the percentage errors of obtained results among all three sets of guess values were less than 1%. The flexural pivot stresses obtained from PRBM and FEA simulation are similar for three different materials of stainless steel, aluminium alloy and polyethylene terephthalate. This indicates that the compliant stretcher mechanism had the potential of achieving the same function regardless of sizes and materials.

References

1. P. Lande. J. Innov, **3**, 53-60 (2014)
2. A. Midha, Bapat, S.G., Mavanthoor, A. and Chinta, V. J. Mech. Robot. **7**, 031007-031010 (2015)
3. L.L. Howell and Midha, A. J. Mech. Des., **116**, 280-290 (1994)
4. L.L. Howell and Midha, A. J. Mech. Des., **117**, 156-165 (1995)
5. J. Crews, Midha, A. and Dharani, L. (2017)
6. M.D. Murphy, Midha, A. and Howell, L.L. , Mech. Mach. theory. **31**, 185-199 (1996)
7. L.L. Howell. pp. 1-13. (2013)
8. M.S. Hajhashemi, Barazandeh, F., Nejad, S.N. and Nadafi Db, R. Proc. Inst. Mech. Eng., Part C, **225**, 2739-2748 (2011)